JOURNAL OF GUIDANCE, CONTROL, AND DYNAMICS
Vol. 31, No. 6, November–December 2008

Haptic Feedback in Uninhabited Aerial Vehicle Teleoperation with Time Delay

T. M. Lam,* M. Mulder,† and M. M. van Paassen‡
Delft University of Technology, 2629 HS Delft, The Netherlands

DOI: 10.2514/1.35340

In the teleoperation of an uninhabited aerial vehicle, haptic feedback can be used to provide useful information through the sense of touch. Although this can improve performance and enhance situation awareness, time delays caused by signal transmission generally induce control problems with haptic feedback, causing unsafe operations. Wave variables have been suggested to cope with the control problems in bilateral human–machine systems with time delay. Very little has been reported, however, on effects related to human control activity and workload when using wave variables. This paper describes a theoretical analysis of using wave variables to enhance a collision-avoidance system for visual and haptic uninhabited aerial vehicle teleoperation with time delay. An experiment was conducted to evaluate its effectiveness regarding operator performance, control activity, workload, and the safety of operation. Results indicate that wave variables are indeed successful in improving human performance. The number of collisions, operator control activity, and workload all decreased. Whereas performance and control activity were equivalent to the situation of haptic feedback without time delay, workload remained higher.

Nomenclature

B_{st}	=	stick damping coefficient, Nms/rad
b	=	characteristic wave impedance, Ns/m
E	=	energy, Nm
F	=	force, N
I_{st}	=	stick moment of inertia, kg m^2
K_{st}	=	stick spring constant, Nm/rad
M	=	moment, Nm
m	=	mass, kg
P	=	power, Nm/s
R	=	wave reflection damping, Ns/m
t	=	time, s
u, v	=	forward- and backward-moving wave variables, $\sqrt{\text{Nm/s}}$
x	=	position, m
$\dot{x}$	=	velocity, m/s
δ	=	stick deflection, rad
$\dot{\delta}$	=	stick deflection rate, rad/s
τ	=	time delay, s

Subscripts

c	=	commanded
diss	=	dissipation
e	=	environment
ext	=	external
h	=	hand
in	=	inflow
m	=	master
s	=	slave
sd	=	slave desired
tot	=	total

Received 27 October 2007; revision received 11 January 2008; accepted for publication 11 February 2008.

*Researcher, Control and Simulation Division, Faculty of Aerospace Engineering, Kluyverweg 1; t.m.lam@tudelft.nl.

†Associate Professor, Control and Simulation Division, Faculty of Aerospace Engineering, Kluyverweg 1; m.mulder@tudelft.nl. Member AIAA.

‡Associate Professor, Control and Simulation Division, Faculty of Aerospace Engineering, Kluyverweg 1; m.m.vanpaassen@tudelft.nl. Member AIAA.

I. Introduction

IN THE teleoperation of uninhabited aerial vehicles (UAVs), operators are physically separated from the vehicle. A ground station equipped with a control interface is used to guide the UAV through the environment. The information provided is usually visual and the operator lacks other sensory information that a pilot of a manned aircraft would normally perceive, such as sound, vibration, and motion. A visual interface, often based on cameras, is generally limited by the camera field of view, which may lead to poor situation awareness and unsafe teleoperation [1,2]. Additionally, the communication between a UAV and a ground station may involve considerable time delays due to signal transmission, contributing to poor efficiency and safety of teleoperation [3,4].

Previous studies showed that presenting additional information, such as tactile cues via a control device by means of haptic feedback, can complement visual information and increases the efficiency and safety of teleoperation [5–15]. For collision avoidance in UAV teleoperation, the focus of our study, Lam et al. [13], investigated the application of haptic feedback to assist operators in guiding the UAV through an obstacle-laden environment. Earlier research evaluated the effectiveness of an artificial force-field (AFF) algorithm [14,15]. Based on onboard sensor data, this artificial force-field maps environmental constraints to repulsive forces that can be used for haptic feedback. These forces provide operators with information about the environment directly as a result from their control deflections. In turn, they can instantly change their control intentions to avoid collision.

No signal-transmission time delays have been considered so far [13,16–18]. However, teleoperation of a UAV that requires communication via a satellite approximately 30,000 km away may involve a round-trip delay of 400 ms. Because of signal-processing time at the ground station and the remote location, the total time delay can even be larger.

In general, when time delays exist in visual feedback, operators can avoid collision through adopting a "move and wait" strategy, which affects the efficiency of teleoperation; however, stability is not an issue [13,19]. In a bilateral system with haptic feedback, on the other hand, the efficiency of teleoperation is often deteriorated considerably by time delays. Because the delayed repulsive forces act on the control device, they cannot be ignored and will be considered by the operator as external disturbances, a situation that

may lead to instabilities [4]. Even small time delays can cause control difficulties [5,20].

Various techniques have been suggested to deal with time delays in teleoperation. Anderson and Spong [5,21] introduced a method using scattering theory to maintain stability by preserving passivity. Niemeyer and Slotine [22,23] reformulated scattering theory and introduced a transformation of power variables into wave variables. This technique can be extended to further improve performance [24] or to deal with varying time delays [25–27]. Wave variables were mainly applied to master–slave systems in which the slave tracks the master velocity or position. The master and slave dynamics may not be identical, but the systems should have the same order. Telesurgery or space teleoperation of a robot arm are examples of such a master–slave system in which the slave should track the master as accurately as possible and provide contact information when the slave makes contact with the remote environment.

This study focuses on teleoperation of a vehicle, which involves an attitude-rate or position-rate control; that is, the master position represents an attitude-rate or position-rate command for the slave. Rather than feeding back the actual forces, as with a teleoperated manipulator in surgery, virtual forces derived from an artificial force field are being fed back.

Dede et al. [28,29] investigated the effects of wave variables applied to a rate-command controlled master–slave system. Results showed that wave variables successfully reduced the effects of time delays. Their study focused on showing differences in overshoot and oscillations around a position constraint. Whereas the tracking performance of the slave is the main concern for many master–slave systems, performance in UAV teleoperation is also judged on operator control activity, operator workload, and vehicle safety.

This paper describes a theoretical and experimental investigation on the use of wave variables for a collision-avoidance system that provides haptic feedback in UAV teleoperation with time delay. Section II gives a brief review of the wave-variable theory [23]. Section III provides an analysis of applying wave variables to various master–slave systems. Section IV discusses offline simulations to show the applicability of wave variables for a collision-avoidance system that provides haptic feedback. Section V discusses a human-in-the-loop experiment that evaluated the effectiveness of using wave variables with a haptic interface for collision avoidance; metrics include vehicle safety, operator performance, control activity, and workload. The paper ends with a discussion on the results and conclusions in Secs. VII and VIII.

II. Wave-Variable Technique

Time delays introduced by signal transmission in teleoperation play an important role in the stability of closed-loop bilateral systems. The use of scattering theory and wave variables is commonly suggested with the objective to maintain stability of a communication channel with time delay [5,30]. Research indicates that the wave-variable technique maintains passivity without the need to know the exact amount of time delay. In fact, the system would become robust to any amount of time delay or phase lag [11,23,28,30]. So far, research on wave variables and time-delayed communication has been conducted mainly with master–slave systems with same-order dynamics, in which the slave tracks the master velocity or position as closely as possible [5,23,24,31].

Vehicle control may involve a rate-command control, however, in which the control deflection from the master is used as a rate command for the vehicle at the remote location. Few have reported about the use of wave variables for such systems [28,29]. This section will review passivity theory and the wave-variable transformation, followed by a comparison of using wave variables for a typical master–slave system with velocity tracking and a master–slave system using rate command.

A. Passivity Theory

Passivity theory can be described by power or energy flow. In general, power can be expressed by any pair of effort and flow variables. Additionally, power can either be stored or dissipated. The power input flow P_{in} is written in terms of velocity $\dot{x}$ and force F:

$$P_{\text{in}} = \dot{x}^T F = \frac{\mathrm{d}E}{\mathrm{d}t} + P_{\text{diss}} \tag{1}$$

where $\mathrm{d}E/\mathrm{d}t$ is the stored power and P_{diss} is the nonnegative dissipated power. Integration of this equation results in an energy equation:

$$\int_0^t P_{\text{in}}\,\mathrm{d}\sigma = \int_0^t \dot{x}^T F\,\mathrm{d}\sigma = E(t) - E(0) + \int_0^t P_{\text{diss}}\,\mathrm{d}\sigma \tag{2}$$

where $E(0)$ represents the initially stored energy. Passivity theory states that a passive system cannot create energy: the energy output must be less than or equal to the sum of the energy input plus the initially stored energy. Note that a negative value represents energy leaving the system.

A property of passivity theory is that a total system is passive if it consists of passive subsystems. Because power is a product of two variables, a difference in phase of these power variables due to time delays affects the passivity of the communication channel, which in turn affects the passivity of the total system. Therefore, a transformation of the power variables into wave variables was introduced to maintain the passivity of the communication channel [22].

B. Wave-Variable Transformation

Wave variables can be used to represent the power variables in an alternative way. Let u define the forward-moving wave variable to the right and let v define the backward-moving wave variable to the left. Figure 1 illustrates a master–slave system with wave transformation in a delayed-communication channel, with the subscripts m and s representing master and slave, respectively. The subscripts h, sd, and e represent operator hand, desired slave, and environment, respectively.

Figure 2 shows the wave transformation block at the master site. The wave variables u and v can be expressed in the velocity $\dot{x}$, the force F, and the characteristic wave impedance b [11,28]. The outputs u and F of the transformation block can be written as

$$u = \dot{x}\sqrt{2b} - v \tag{3}$$

and

$$F = \dot{x}b - v\sqrt{2b} \tag{4}$$

Reordering Eq. (4) and substituting it into Eq. (3) yields equations for the wave variables u and v in terms of $\dot{x}$ and F:

$$u = \frac{b\dot{x} + F}{\sqrt{2b}} \qquad v = \frac{b\dot{x} - F}{\sqrt{2b}} \tag{5}$$

Equation (5) can be used to substitute the velocity $\dot{x}$ and the force F in power equation (1). This results in a redefinition of the power flow based on the input and output wave variables:

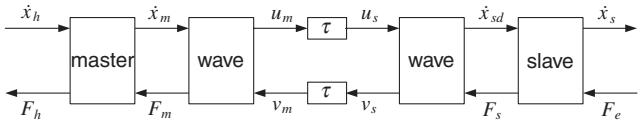

Fig. 1 Communication between master and slave using wave variables.

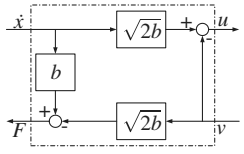

Fig. 2 Wave transformation of the velocity and force into u and v.

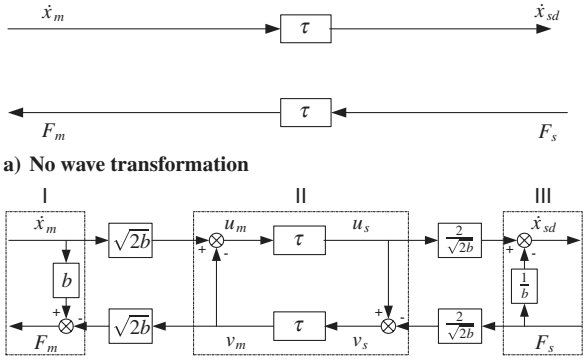

a) No wave transformation

b) Wave transformation in the communication channel

Fig. 3 Signal transmission without (top) and with (bottom) wave transformation.

$$P_{\text{in}} = \dot{x}^T F = \tfrac{1}{2}u^T u - \tfrac{1}{2}v^T v \tag{6}$$

Clearly, the relation between the wave variables in the power equation is not a multiplication, but has become a summation, and passivity is therefore less sensitive to distortion in the signal (e.g., due to time delays). When considering u as the incoming and v as the outgoing wave variables, then according to passivity theory, the energy equation (6) states that the outgoing energy cannot be more than the incoming energy plus the initially stored energy:

$$\int_0^t \frac{1}{2} v^T v \, \mathrm{d}\sigma \le \int_0^t \frac{1}{2} u^T u \, \mathrm{d}\sigma + E(0) \tag{7}$$

Figure 3b shows a detailed representation of a delayed-transmission channel, using wave transformation from Eq. (5) at the master and slave sites.

C. Wave Reflections

Figures 3a and 3b illustrate that in addition to the force feedback from the slave to the master (the aim of the haptic feedback design), the wave transformation introduces several inner-feedback paths. The inner feedback of $\dot{x}_m$ at the master site through the wave impedance b, indicated by block I, serves as damping of the operator control input and is not affected by time delay. The second feedback path, indicated by block II, involves a circulation of wave variables through the delayed-communication channel that results in wave reflections. This becomes clear when rewriting Eq. (5) applied to master and slave, respectively:

$$\begin{aligned} u_m &= \frac{b\dot{x}_m + F_m}{\sqrt{2b}} = \sqrt{2b}\dot{x}_m - v_m \\ v_s &= \frac{b\dot{x}_{sd} - F_s}{\sqrt{2b}} = u_s - \sqrt{\frac{2}{b}}F_s \end{aligned} \tag{8}$$

The waves u_m and v_s contain returning waves v_m and u_s, respectively. The wave reflection does not contain much useful information. Additionally, it may cause undesired oscillations, leading to control difficulties. It was therefore suggested by Niemeyer and Slotine [23] to minimize the wave reflections through eliminating the returning waves using an impedance-matching technique or wave filters. The impedance-matching technique will be discussed in Sec. IV.A. The third feedback, indicated by block III, involves immediate feedback of the repulsive force F_s to the slave at the remote site. Therefore, the response of the slave does not completely depend on the delayed response of the operator; that is, when the operator perceives the repulsive force, the slave has already started to move in a direction that corresponds to the repulsive force.

III. Master–Slave Systems

Wave variables are commonly used in research on teleoperation involving master–slave systems with time delay [23,26,27,31]. Our study focuses on teleoperating a UAV helicopter in which the control deflection from the haptic device represents a velocity command for the UAV. Hence, the control law differs from that of a typical master–slave system. In this section, the application of wave variables to a conventional master–slave system and to a rate-command system, representative for UAV teleoperation, will be discussed.

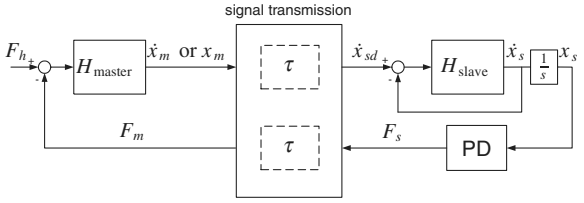

Fig. 4 Schematic representation of a master–slave system; for velocity-tracking and rate-command systems, the master output is $\dot{x}_m$ and x_m, respectively.

A. Velocity-Tracking Master–Slave System

Consider a simple system with velocity tracking by the slave (Fig. 4). Both the master and slave are modeled as a mass between the force input and velocity output, $(1/m_m)\cdot(1/s)$ and $(1/m_s)\cdot(1/s)$, respectively. Both masses are 1 kg. The master velocity $\dot{x}_m$ is transmitted through the signal-transmission block as a desired slave velocity $\dot{x}_{\text{sd}}$. The actual slave velocity $\dot{x}_s$ is used for an inner-feedback loop to track the master velocity. The slave position x_s, with respect to its initial position 0 m (environment constraint), serves as input to a proportional–derivative (PD) controller to generate force feedback F_s, where $P = 0.5$, $D = 2$, F_m is the force reflected to the master, and F_h is the force exerted by the operator. The communication time delay $\tau = 0.2$ s is modeled by a second-order Padé approximation.

Simulations with a step input on F_h are conducted with three configurations: 1) no time delay, our baseline; 2) time delay without wave variables; and 3) time delay with wave variables. Figures 3a and 3b show detailed representations of the signal-transmission block from Fig. 4 for no wave variables and wave variables, respectively.

Figure 5a shows the system response for the three configurations. Without wave variables, the response becomes unstable, whereas using wave variables, the response is similar to the system response with no time delay. The energy flow through the communication channel, measured using the passivity observer suggested by Hannaford and Ryu [32], is shown in Fig. 5b. The energy flow is zero and positive for the no-delay and the wave-variable configurations, respectively; that is, both are passive subsystems. The configuration without wave variables has negative energy, indicating a nonpassive communication system. Figure 5c shows a root locus as a function of the characteristic wave impedance b for $\tau = 0.1, 0.2$, and 0.5 s. It can be seen that the velocity-tracking master–slave system remains stable when b increases. The poles approach the imaginary axis asymptotically, independent of the delay time.

B. Rate-Command Master–Slave System

UAV teleoperation may involve a rate-command control in which the control deflection from the master is used as a rate command for the vehicle at the remote location. The system is shown in Fig. 4; a similar system was used by Dede et al. [28].

Here, the master stick deflection x_m is transmitted as a velocity command for the slave. The master and slave dynamics differ from each other. The master is modeled as a mass-spring-damper system between the force input and the deflection output:

$$H_{\text{master}} = \frac{1}{0.01s^2 + 0.2s + 2}$$

The slave is modeled as a mass of 0.5 kg between the control input and the slave velocity output:

$$H_{\text{slave}} = \frac{1}{0.5}\cdot\frac{1}{s}$$

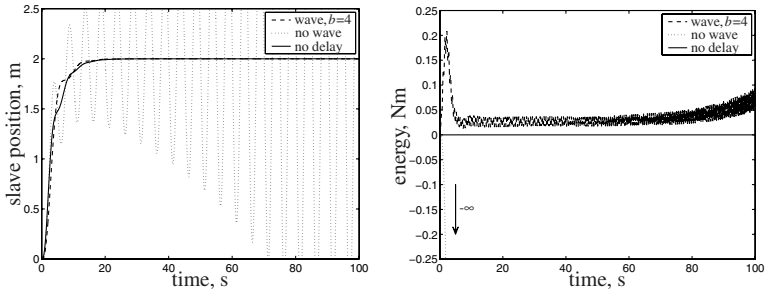

a) Position response b) Energy response

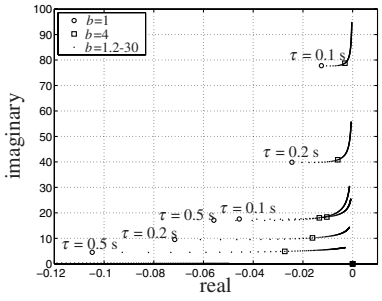

c) Root locus

Fig. 5 Time response of the slave position, energy over the communication channel, and root locus for a velocity-tracking system.

The slave position serves as input to the PD controller in Fig. 4 with $P = 0.3$ and $D = 0.9$. The configurations and time delay were the same as in Sec. III.A.

The time response in Fig. 6a shows that also for the rate-command system, even a small time delay of 0.2 s will cause large oscillations in the slave position. Wave variables reduce the instability effects and the response becomes similar to the one with no time delay. The energy is also measured using the passivity observer, with the master flow variable x_m representing the velocity command from the master. Again, Fig. 6b shows that no time delay and wave variables result in a passive communication system, whereas without wave variables, the energy is negative, corresponding to a nonpassive system. The root locus in Fig. 6c shows that the system remains stable for certain values of the wave impedance b. The poles will eventually leave the left half of the s plane for increasing values of b, resulting in an unstable system.

From the preceding, it is clear that a rate-command master–slave system can be combined with the wave-variable technique to reduce the effects of time delays. The simulations, however, are based on linear feedback of the slave position and velocity for generating force feedback and the input is constant. In our application, a collision-avoidance system in the UAV teleoperation, a nonlinear artificial force field is used to generate repulsive forces. The operator inputs also change during flight. Additionally, whereas the simulations focused on the slave behavior when approaching a steady-state position, for collision avoidance, it is important that position constraints should not be exceeded. These effects will be investigated in the next section.

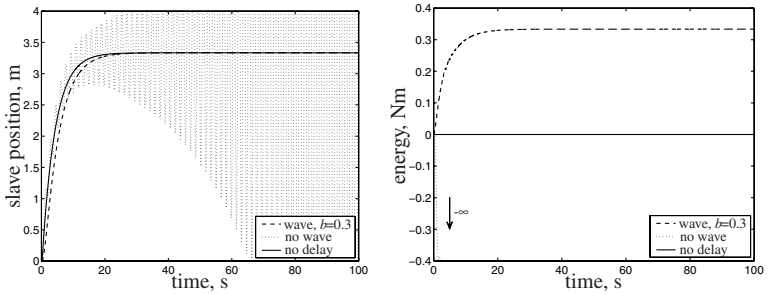

a) Position response b) Energy response

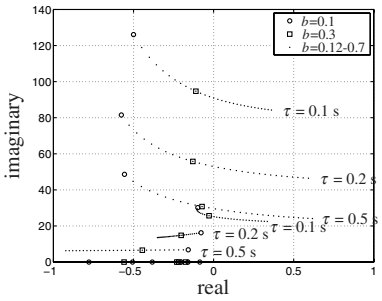

c) Rate command system

Fig. 6 Time response of the slave position, energy over the communication block, and root locus for a rate-command system.

IV. Offline Simulations of UAV Teleoperation

This section describes offline simulations in which a UAV flew through an environment with obstacles. The task was to move from an initial position to a target position without collisions. The goal of the simulations was to investigate whether wave variables can be used for UAV teleoperation that incorporates a rate-command control system and an artificial force field. Important aspects are the UAV motion and the collision-avoidance effectiveness.

A. Setup

Figure 7 shows a schematic representation of the closed-loop system. The model contains an autopilot that represents linear human-operator control dynamics. It also consists of a stick control device, UAV dynamics, and an artificial force field. Next, the components of the model will be described in more detail.

The autopilot H_{ap} is a PD controller on the position error with respect to the target position. The output of the autopilot serves as moment input M_c to the stick control device. The stick H_{stick} is modeled as a mass-spring-damper system with moment of inertia $I_{\text{st}} = 0.01$ kg m^2, damping coefficient $B_{\text{st}} = 0.2$ Nms/rad, and spring constant $K_{\text{st}} = 2$ Nm/rad. The stick deflection δ_c serves as a velocity command for the UAV model. The UAV H_{UAV} is assumed to be control-augmented with equivalent dynamics $2/(s+2)$ between the commanded velocity and the actual velocity output. The UAV is modeled to have a maximum velocity of 5 m/s and a maximum acceleration of 1 m/s^2.

The AFF is used to map obstacles to repulsive forces. Both the parametric risk field and the basic risk field from Lam et al. [15] are evaluated. The parameters of the parametric risk field are $d_{\min} = 1.5$ m and $t_{\text{ahead}} = 2$ s. The scale factor of the basic risk field is $K = 10$. Note that for a detailed description of these two artificial force fields and their parameters, the reader is referred to Lam et al. [15].

An integrated sensor that scans the environment 360 deg with an angular resolution of 3 deg and a range of 50 m is simulated. The repulsive-force vectors generated by the AFF point along the sensor radial lines.

The control input and haptic feedback are subjected to a transmission time delay $\tau = 0.2$ s. When wave variables are not used, the signal-transmission block is represented by Fig. 3a, whereas Fig. 3b represents the signal transmission using wave variables with $b = 0.3$ Ns/m. The visual feedback is also subjected to the same time delay, but in all cases, no wave variables are applied to this feedback channel.

To prevent control difficulties due to oscillations caused by wave reflections, impedance-matching with the addition of an explicit matched termination is used to minimize the reflections [22]. A damping R with a value equal to b is used at the slave site (see Fig. 8). The purpose of the damping R is to eliminate the reflected wave u_s in the returning wave v_s in Eq. (8). Because u_s is encoded in $\dot{x}_{\text{sd}}$, feedback of $\dot{x}_{\text{sd}}$ through $R = b$ will eliminate u_s, and no circulation of u_s in the delayed communication will occur.

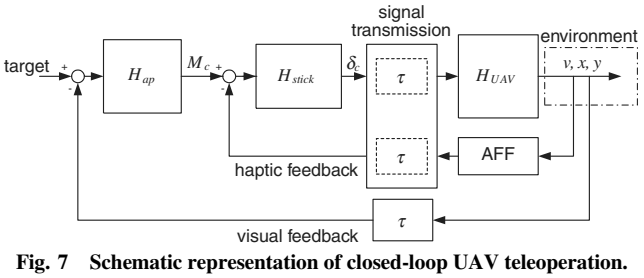

Fig. 7 Schematic representation of closed-loop UAV teleoperation.

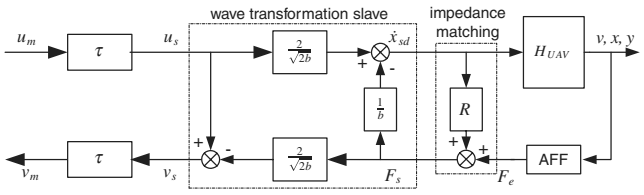

Fig. 8 Wave transformation at the slave site with wave impedance matching.

B. Environment

The same trajectories are used as in Lam et al. [15], and they are shown in Figs. 9 and 10. The start and target positions are represented by ○ and ⋆, respectively, with an alphabetic character indicating the corresponding trajectory. The dashed circles with 1-s intervals indicate the UAV position, and the arrows represent the repulsive forces. Maneuvers such as making a sharp turn, a passage through narrow corridors, stopping before a dead end, and moving through a passage with irregularities in the wall are used to test the efficiency of the AFF with time delay.

C. Results

Figure 9 illustrates that without wave variables, teleoperation with time delay becomes very difficult. Particularly, in trajectories A, B, and D, which require special maneuvers, oscillations in the repulsive-force vectors and UAV motion occur and result in collisions. In trajectory C the UAV can still stop in front of a straight wall for both AFFs.

Figure 10 shows that using wave variables provides almost the same results as those found in the previous study with no time delay [15]. The reduction in oscillations corresponds well to the findings in Sec. III.B. Use of wave variables again yields a well-damped slave response.

The simulations were conducted with a simple model of the operator dynamics. In practice, time delays in both the visual and the force-feedback channels affect the operator control strategy, efficiency, and performance. Because the delayed repulsive forces act directly on the control device and may lead to instability, delayed haptic feedback is more critical than delayed visual feedback. Because time-delay effects on force feedback have been shown to be reduced significantly with wave-variable formulations, it is important to investigate whether this improvement still holds with an operator in the loop and whether operator control strategy, efficiency, and performance will change.

V. Human-in-the-Loop Experiment

An experiment was conducted to investigate the effects of using wave variables with a collision-avoidance system in the teleoperation of a UAV. The investigation focused on collision avoidance, operator performance, control activity, and workload.

A. Method

1. *Subjects and Instructions*

Nine subjects aged 24 to 29, with no flight experience, participated. Their main task was to fly from waypoint to waypoint as fast as possible and to move through the center of the waypoint as accurately as possible. The experiment simulated a reconnaissance task in a hazardous environment. Waypoints were represented by smoke plumes located in the vicinity of an obstacle. Subjects were not provided with information as to whether or when a collision occurred. After each run, subjects were asked to rate their workload using the NASA task-load index (TLX) rating scale [33], which assumes operator workload to be contributed by six sources: mental demand, physical demand, temporal demand, performance, effort, and frustration level. First, subjects needed to choose between each pair of the six sources that contributed most to their workload. Second, each source was given a rating using a scale from low to high, except for the performance, which was rated using a scale from good to bad.

In addition to the TLX rating scale, a questionnaire after each run was used to assess subject experience with the control configuration. The questionnaire complemented the results from the TLX. The questions were split into two categories: mental workload and

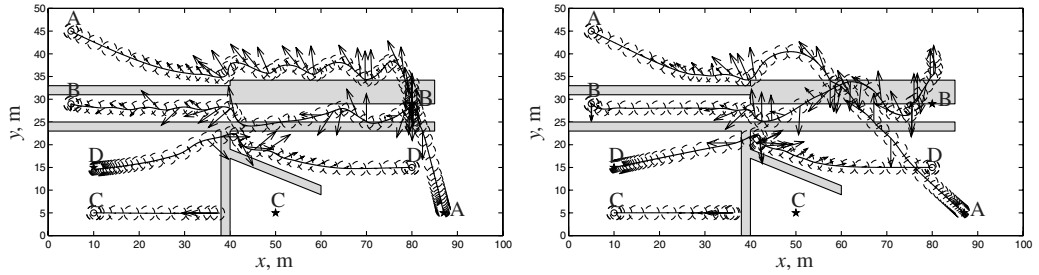

a) Basic risk field b) Parametric risk field

Fig. 9 UAV trajectories without wave variables.

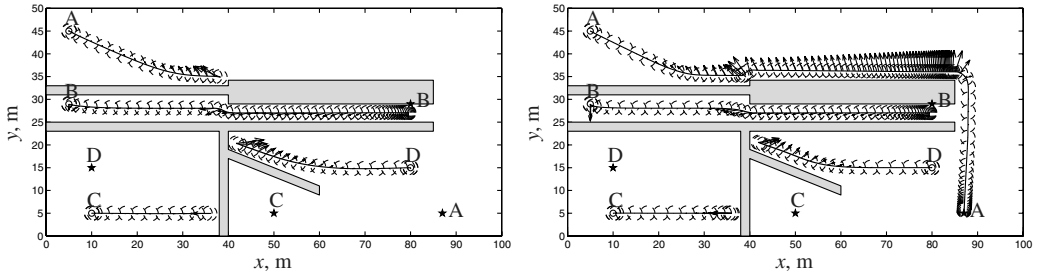

a) Basic risk field b) Parametric risk field

Fig. 10 UAV trajectories with wave variables.

physical workload. The mental-workload-related questions considered 1) the difficulty of estimating the time to initiate an avoidance maneuver, 2) the difficulty of being aware of a dangerous approach toward an obstacle, and 3) the difficulty of being aware of a collision.

The physical-workload-related questions considered 1) the required physical effort to fly through closely spaced obstacles, 2) the need to counteract the repulsive forces in case of haptic feedback, and 3) the comfort of teleoperation.

2. *Apparatus*

The experiment was conducted in a fixed-base flight simulator. Subjects were seated in front of an 18-in. screen, representing a navigation display, as shown in Fig. 11a. A simulated onboard camera outside visual display was projected on a wall at a distance of 2.9 m in front of the operator, as shown in Fig. 11b. The horizontal and vertical fields of view of the camera were 60 and 45 deg, respectively.

On the right-hand side of the chair, an electrohydraulic side stick was used as the haptic control device. The mass-spring-damper stick dynamics were simulated with inertia $I_{st} = 0.01$ kg m^2, damping coefficient $B_{st} = 0.2$ Nms/rad, and spring constant $K_{st} = 2$ Nm/rad, defined at 0.09 m above the rotation axis, which is approximately the position of the hand contact point. The stick dynamics were identical for the lateral and longitudinal axes.

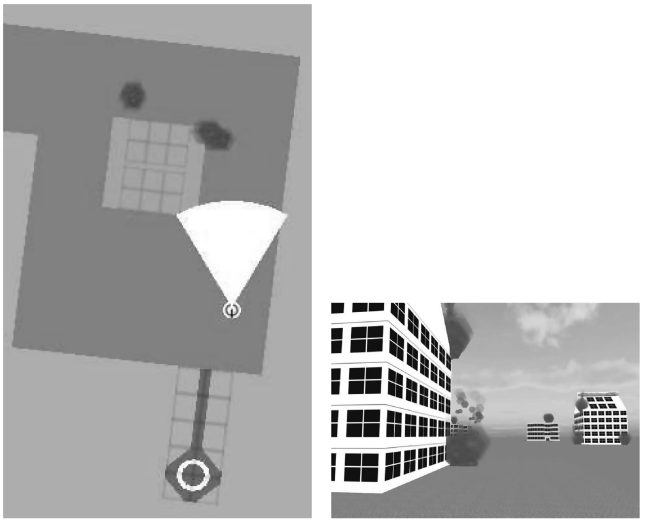

a) Navigation display b) Camera display

Fig. 11 Visual displays used in the experiment.

3. *UAV Model*

A control-augmented UAV helicopter model was used [34]. A stick deflection in the longitudinal direction represented a velocity command V_x, and a stick deflection in the lateral direction generated a yaw rate rotation $\dot{\psi}$ along the z axis, all with respect to a rotating geodetic-axis system, as shown in Fig. 12. The helicopter model had a maximum velocity of 5 m/s and a maximum acceleration of 1 m/s^2. Altitude was kept constant at 3.5 m. The UAV had a circular protection zone with a radius of 1.6 m; any object within this zone was considered to collide with the UAV.

4. *Independent Variables*

Five levels of control interface configurations (CF) were used:

1) BL indicates no haptic feedback with no time delay (baseline).
2) DL indicates no haptic feedback with time delay.
3) HF indicates haptic feedback with no time delay.
4) HFDL indicates haptic feedback with time delay.
5) WV indicates haptic feedback with time delay and wave variables.

The time delay was fixed at 0.2 s; the wave-variable impedance was set at $b = 0.3$ Ns/m.

Six subtasks (ST) were used involving different scenarios, each requiring a specific maneuver that may lead to control difficulties.

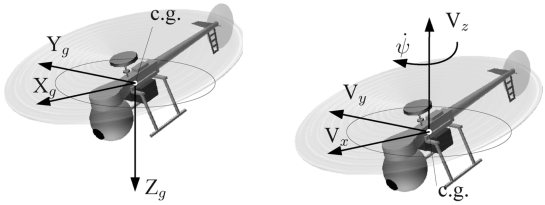

a) Rotating geodetic axis frame b) Helicopter commands

Fig. 12 Reference frames of the UAV model.

The subtasks are illustrated in Fig. 13, with an arrow showing the initial flight direction and stars indicating the locations of the waypoints represented by the smoke plumes. Note that a secondary purpose of the smoke plumes was to reduce the visibility of the boundaries of obstacles in the vicinity, emphasizing the haptic feedback when active.

In subtask 1, the helicopter had to make a 90-deg turn around a building, as shown in Fig. 13a. Before the turn, the UAV had to approach the first waypoint, forcing the UAV to fly closely to the corner. The second waypoint was located after the corner to stimulate subjects to turn as sharply as possible.

In subtask 2, the helicopter was to fly through a narrow gate in which the pillars served as two closely spaced, small obstacles. Figure 13b shows a cross section of the gate. The smoke at the waypoint reduced the visibility of the pillar boundaries.

For subtask 3, once the helicopter had reached the diamond, it should have hovered backward toward the building until the operator saw a stop sign that was below the flight altitude and fixed in the world (asterisk), as depicted in Fig. 13c. Hence, the camera did not point in the direction of motion and it was expected that haptic feedback would become very useful. Moreover, smoke appearing from the top of the building reduced the visibility of the building edges.

The 4 scenario consisted of a building with a discrete change in the shape of the wall. The first waypoint was located before this change and forced the UAV to approach the wall, followed by an escape maneuver to avoid collision with the extension of the wall in Fig. 13d. The second waypoint forced the UAV to stay close to the building during the escape maneuver.

In subtask 5, two buildings with discrete changes in opposite directions could lead to oscillatory behavior in the stick and considerable control difficulties. The first waypoint on the right would force the UAV to make a sharp turn, whereas the second waypoint on the left would force the UAV to make an escape maneuver, as shown in Fig. 13e.

In subtask 6, the turn radius with haptic feedback would be limited due to the obstacles in front and on the left-hand side. It was expected that this subtask would lead to control difficulties, especially when approaching with high speed. The first waypoint on the left forces the UAV to approach the side of the left building whereas the second waypoint forces the UAV to make a quick turn to fly closely along the corner of the right building. The third waypoint would force the UAV to approach another wall after the turn shown in Fig. 13f.

Table 1 Order of subtasks inside each sector used in the trajectories

Sector	Subtask order
1	1-2-3-4-6-5
2	3-1-4-5-6-2
3	4-1-5-3-2-6

5. Trajectory

In general, the trajectories (scenarios) were the same as those used by Lam et al. [13]. The main difference was the lack of presenting a reference trajectory in this experiment. For navigation purposes, the subtask areas had a darker background color on the navigation display (see Fig. 11a). Five trajectories were designed, with each trajectory containing three sectors [13] and each sector containing the six subtasks in a different order. Table 1 shows the sectors and the corresponding order of the subtasks. A trajectory thus contained three repetitions of each subtask and was flown once for each of the five control interface conditions. Hence, subjects flew $5 \times 5 = 25$ runs, each lasting approximately 6 min. Figure 14 shows an example trajectory.

6. Procedure

Before the measurements, subjects got the opportunity to get familiar with the five control configurations. Then each subject flew the 25 experiment runs in a random order. There were three random orders, with three subjects flying each order. Subjects were not informed about which condition they flew during the measurement runs.

B. Dependent Measures

Operator control activity was represented by the standard deviation and the mean of the total exerted moment by the hand (σ_{M_h} and $\bar{M}_h$) and the standard deviation of the total stick deflection rate ($\sigma_{\dot{\delta}_{\text{tot}}}$). Haptic activity was represented by the standard deviation and the mean of the total *external* moment by the haptic device ($\sigma_{M_{\text{ext}}}$ and $\bar{M}_{\text{ext}}$). Operation efficiency was represented by the standard deviation of the total speed and the elapsed time ($\sigma_{v_{\text{tot}}}$ and T_{el}). The level of safety was expressed by the number of collisions and the minimum distance toward an obstacle, $D_{\min}$ (in meters). Operator performance was expressed by the minimum distance from the

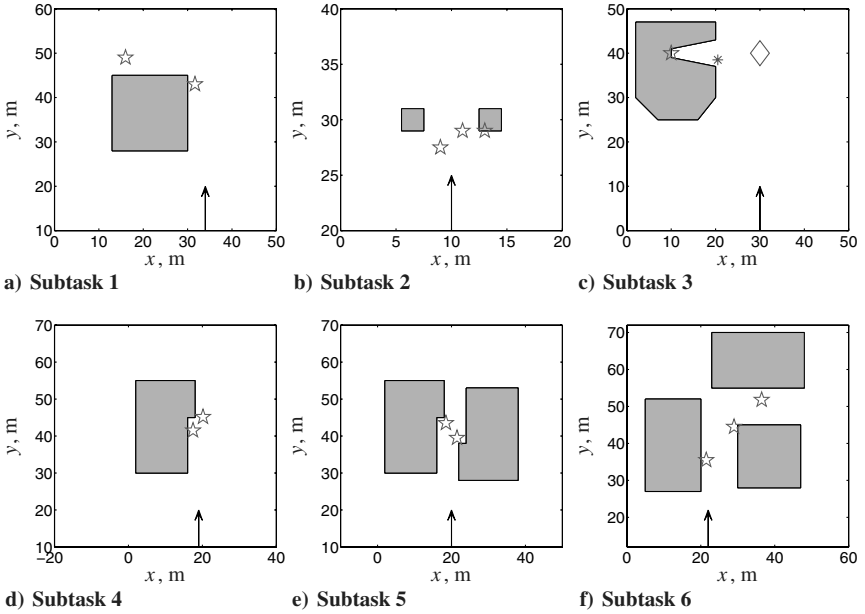

Fig. 13 Six subtasks used in the experiment.

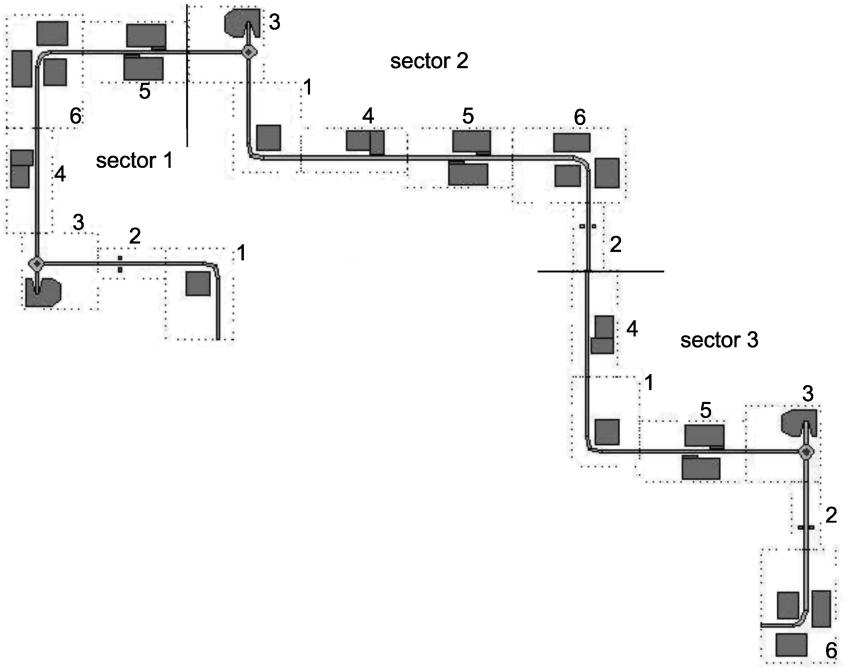

Fig. 14 Example trajectory, with three repetitions of the six subtasks.

smoke location, D_{smoke} (in meters). Operator workload and situation awareness were measured after each run using the NASA TLX rating scale and the questionnaire, respectively.

C. Hypotheses

First, it was hypothesized that with haptic feedback safety, operator control activity and workload will increase with respect to the baseline condition. Second, it was hypothesized that time delay in haptic feedback would result in a decrease in safety and a further increase in control activity and workload. Third, it was hypothesized that these deteriorating effects with haptic feedback caused by the time delay would be reduced considerably using wave variables.

VI. Results

The main results are discussed in this section. A full-factorial within-subjects analysis of variance was applied with posthoc analyses using Student–Newman–Keuls ($\alpha = 0.05$). Table 2 summarizes the analysis of variance results. The subjective data (i.e., workload ratings and questionnaire answers) were analyzed using Kruskal–Wallis tests followed by Mann–Whitney tests to find the configurations that were significantly different. Figures 15 and 16 show the number of collisions. The means and 95%-confidence intervals of the other dependent measures are shown in Fig. 17. The medians and interquartile ranges of the subjective measures are shown in Figs. 18 and 19.

A. Objective Data

1. Collisions

Figure 15 shows that the number of collisions was largest for BL and DL. HF resulted in a considerable reduction of collisions, also reported by Lam et al. [17]. A Kruskal–Wallis test revealed a highly significant effect of the configuration ($\chi^2 = 107.009$ and $p \leq 0.01$). When haptic feedback was used with time delay, however, the number of collisions increased. Mann–Whitney tests revealed that wave variables resulted in a highly significant reduction in the number of collisions. The number of collisions was even smaller than with HF (i.e., *without delay*): $Z = -3.863$ and $p \leq 0.01$.

Mann–Whitney tests also revealed that subtask 5 resulted in the largest number of collisions, followed by subtask 3 (see Fig. 16). The lowest amount of collisions was observed in subtasks 2 and 4. Subtask 1 resulted in more collisions than subtask 4, although the subtask was considered beforehand to be relatively simple. Subjects flew more cautiously, with a larger distance to the obstacles (see also Sec. VI.A.4) in subtask 4, whereas in subtask 1, corner-cutting contributed to the large number of collisions.

For subtasks 3, 5, and 6, with closely spaced obstacles surrounding the UAV, Mann–Whitney tests revealed that WV resulted in a significantly smaller number of collisions than with DL and HFDL. Surprisingly, in subtask 2 with a relatively simple task and in subtasks 1 and 4 with an obstacle at one side of the UAV, DL resulted in less collisions than with BL, although not significantly. And in subtasks 1 and 4, HFDL did not result in a larger number of collisions than with HF. These effects may be attributed to the fact that with an obstacle at just one side, subjects flew more cautiously when there was a time delay and the UAV remained at a larger distance from the obstacle, yielding less collisions. Such a strategy could not be applied, however, in subtasks 2, 3, 5, and 6, in which the UAV was surrounded by obstacles on both sides.

2. Control Activity

Control activity in terms of the standard deviation of the total operator-exerted moment on the stick (σ_{M_h} in Fig. 17a) was largest with HFDL and smallest with BL, a highly significant effect

Table 2 Results of a full-factorial analysis of variance of the main dependent measures[a]

Variable	Control activity $\sigma_{\dot{\delta}_{\text{tot}}}$	σ_{M_h}	$\bar{M}_h$	Haptic activity $\sigma_{M_{\text{ext}}}$	$\bar{M}_{\text{ext}}$	Speed $\sigma_{v_{\text{tot}}}$	Approach performance D_{smoke}	Minimum distance D_{min}	Elapsed time T_{el}
Main effects									
CF	⋆⋆	⋆⋆	⋆⋆	⋆⋆	⋆⋆	⋆⋆	⋆⋆	⋆⋆	⋆⋆
ST	⋆⋆	⋆⋆	○	⋆⋆	⋆⋆	⋆⋆	○	⋆⋆	——
Two-way interactions									
CF × ST	⋆⋆	⋆⋆	⋆⋆	⋆⋆	⋆⋆	⋆⋆	⋆⋆	⋆⋆	⋆⋆

[a]The symbols ⋆⋆ and ○ represent chance levels of $p \leq 0.01$ and $0.05 < p \leq 0.10$, respectively.

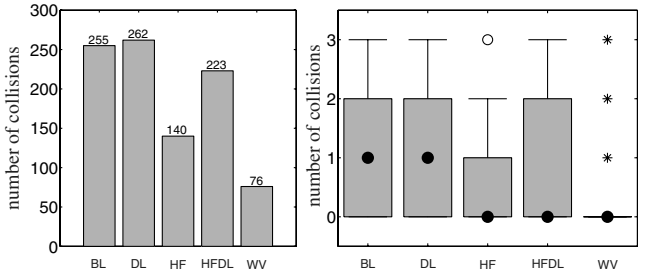

a) Total number of collisions

b) Medians and interquartile ranges of the number of collisions with medium (○) and severe (∗) outliers

Fig. 15 Number of collisions.

(CF: $F_{4,32} = 23.012$ and $p \leq 0.01$). No significant difference in σ_{M_h} between HF and WV was found in most of the subtasks. Regarding the dependency on ST, subtask 2 resulted in the smallest σ_{M_h} and subtask 3 resulted in the largest σ_{M_h}, a highly significant effect (ST: $F_{5,40} = 27.697$ and $p \leq 0.01$). In subtask 6, WV even resulted in smaller σ_{M_h} than with HF, which led to the highly significant two-way interaction (CF × ST: $F_{20,160} = 6.603$ and $p \leq 0.01$). The mean exerted moment in Fig. 17b was smallest with BL and largest with HFDL and WV (CF: $F_{4,32} = 25.472$ and $p \leq 0.01$).

Figure 17c shows that BL resulted in the smallest standard deviation of the total stick deflection rate, $\sigma_{\dot{\delta}_{\text{tot}}}$, whereas HFDL resulted in the largest $\sigma_{\dot{\delta}_{\text{tot}}}$, a highly significant effect (CF: $F_{4,32} = 30.358$ and $p \leq 0.01$). Again, HF and WV resulted in equivalent $\sigma_{\dot{\delta}_{\text{tot}}}$ in most subtasks, except in subtask 5, in which WV resulted in a larger $\sigma_{\dot{\delta}_{\text{tot}}}$ than with HF. Subtask 2 involved a simple task with forward flight and resulted in the smallest $\sigma_{\dot{\delta}_{\text{tot}}}$, whereas subtask 5 involved a difficult approach and avoidance maneuver, which resulted in the largest $\sigma_{\dot{\delta}_{\text{tot}}}$, a highly significant effect (ST: $F_{5,40} = 18.409$ and $p \leq 0.01$).

3. Haptic Activity

Here, BL and DL are not considered because they did not provide any haptic forces. Figure 17d shows that WV resulted in the smallest standard deviation of the external moment on the stick, whereas HFDL resulted in highest haptic activity, a highly significant effect (CF: $F_{2,16} = 103.016$ and $p \leq 0.01$). Subtask 1 resulted in the lowest haptic activity, whereas subtasks 5 and 6 with closely spaced buildings resulted in the highest haptic activity (ST: $F_{5,40} = 37.239$ and $p \leq 0.01$).

The mean external moment in Fig. 17e was smallest with HF and largest with WV, a highly significant effect (CF: $F_{2,16} = 19.690$ and $p \leq 0.01$). Subtasks 1 and 5 resulted in the lowest and highest $\bar{M}_{\text{ext}}$, respectively, a highly significant effect (ST: $F_{5,40} = 46.251$ and $p \leq 0.01$). In subtask 3, HFDL resulted in the largest $\bar{M}_{\text{ext}}$, which resulted in a highly significant two-way interaction (CF × ST: $F_{10,80} = 29.904$ and $p \leq 0.01$).

4. Minimum Distance

Figure 17f shows that BL and DL resulted in the smallest distances to obstacles followed by HFDL; WV resulted in the largest distances, a highly significant effect (CF: $F_{4,32} = 37.758$ and $p \leq 0.01$). Note that the negative values of the minimum distance in subtasks 3 and 5 for BL, DL, and HFDL correspond to the large number of collisions discussed in Sec. VI.A.1. They also indicate that in subtasks 3 and 5, collisions nearly always occurred, except for HF (no delay) and WV (with delay). This clearly demonstrates the effectiveness of haptic feedback.

Regarding the influence of the subtask, the minimum distance was smallest in subtask 5, followed by subtasks 3 and 6, all involving obstacles at both sides of the UAV. The largest distance was observed in subtask 4, followed by subtask 1, both involving an obstacle at one side of the UAV, a highly significant effect (ST: $F_{5,40} = 37.515$ and $p \leq 0.01$).

5. Speed

The standard deviation of the total speed, $\sigma_{v_{\text{tot}}}$, in Fig. 17g was smallest with BL and largest with HFDL and WV, a highly significant effect (CF: $F_{4,32} = 7.916$ and $p \leq 0.01$). Subtask 2 resulted in the smallest $\sigma_{v_{\text{tot}}}$; subtask 3 resulted in the largest $\sigma_{v_{\text{tot}}}$, a highly significant effect (ST: $F_{5,40} = 34.489$ and $p \leq 0.01$). In subtask 3, WV resulted in the smallest $\sigma_{v_{\text{tot}}}$ which resulted in a highly significant two-way interaction (CF × ST: $F_{20,160} = 4.143$ and $p \leq 0.01$).

6. Elapsed Time

The elapsed time was smallest with BL, DL, and HF and was largest with HFDL and WV, a highly significant effect (CF: $F_{4,32} = 18.530$ and $p \leq 0.01$). For the elapsed time, no comparison was made between subtasks, due to differences in trajectory lengths.

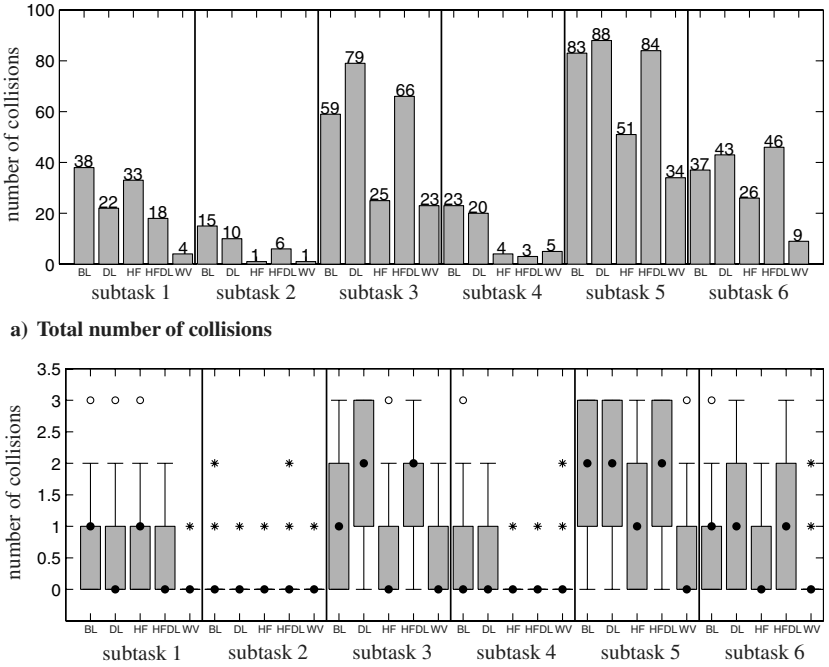

a) Total number of collisions

b) Medians and interquartile ranges of the number of collisions with medium (○) and severe (∗) outliers

Fig. 16 Number of collisions clustered for each subtask.

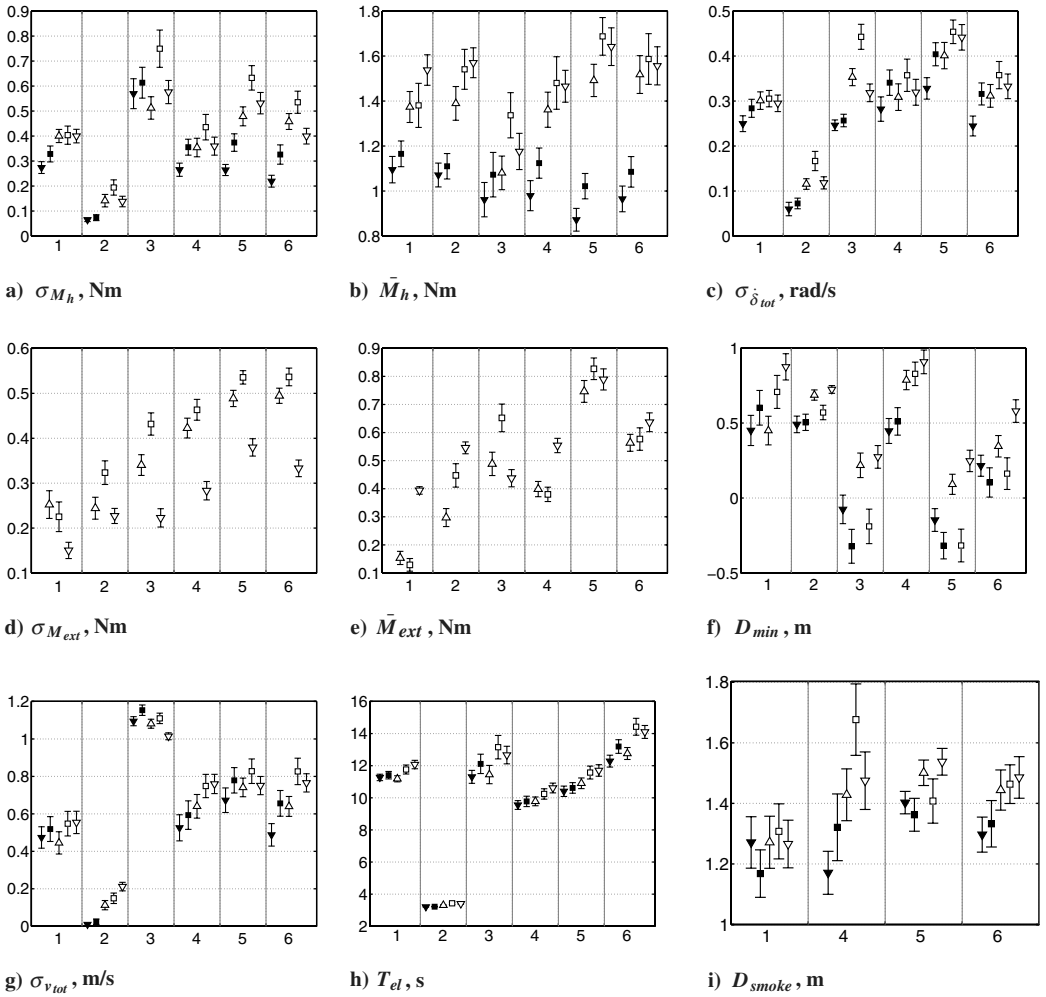

Fig. 17 Means and 95% confidence intervals of the main dependent measures: BL (filled triangle), DL (filled square), HF (open up triangle), HFDL (open square), and WV (open down triangle); numbers on the horizontal axis represent the six subtasks.

7. Approach Performance

For performance in terms of the minimum distance from the smoke, subtasks 2 and 3 were not considered, because the smoke in those subtasks only served as "noise" in the visual information of the obstacle boundaries, rather than as a waypoint. Figure 17i shows that, as was hypothesized, the three haptic feedback configurations HF, HFDL, and WV all resulted in larger distances from the smoke than the configurations without haptic feedback, a highly significant effect (CF: $F_{4,32} = 10.800$ and $p \leq 0.01$).

B. Subjective Data

1. TLX Workload

Because workload was measured after a full run, the effects of the subtask could not be measured. Figure 18 shows the median and dispersion of the rated TLX workload. A Kruskal–Wallis test revealed a highly significant effect of the configuration on workload ($\chi^2 = 50.692$ and $p \leq 0.01$). Mann–Whitney tests revealed that workload was highest with HFDL and lowest with BL.

2. Questionnaire

The estimation of the time to initiate an avoidance maneuver was considered to be the most difficult with DL and HFDL (Fig. 19a). HF resulted in the least difficulty, whereas WV and BL were in-between, a highly significant effect (CF: $\chi^2 = 46.625$ and $p \leq 0.01$). The awareness of a dangerous approach toward an obstacle was reported to be the least difficult with HF, whereas DL was considered to be the most difficult (Fig. 19b). BL, HFDL, and WV were rated in-between, a highly significant effect (CF: $\chi^2 = 52.143$ and $p \leq 0.01$). The awareness of a collision was higher for all three haptic feedback configurations: HF, HFDL, and WV (Fig. 19c). Awareness was low without tactile cues BL and DL, a highly significant effect (CF: $\chi^2 = 51.530$ and $p \leq 0.01$).

The physical effort in flying between closely spaced obstacles was lowest with BL, followed by DL (Fig. 19d). HFDL resulted in the largest effort, followed by WV and HF, a highly significant effect (CF: $\chi^2 = 173.343$ and $p \leq 0.01$).

The analysis of the necessity to counteract the repulsive forces was done without DL and BL, because they did not provide repulsive forces. Figure 19e shows that HFDL resulted in the highest need to counteract the repulsive forces, whereas WV and HF resulted in the lowest need for counteracting, a highly significant effect (CF: $\chi^2 = 33.383$ and $p \leq 0.01$). The comfort of flying was highest with BL. The lowest comfort of flying was with HFDL, a highly significant effect (CF: $\chi^2 = 65.209$ and $p \leq 0.01$). WV did not result in less comfort than with HF, the situation without delay (see Fig. 19f).

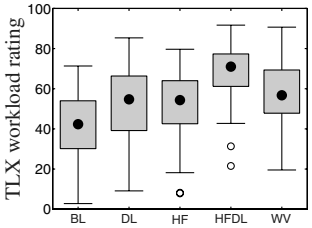

Fig. 18 Medians and interquartile ranges of the TLX workload rating with medium (○) outliers.

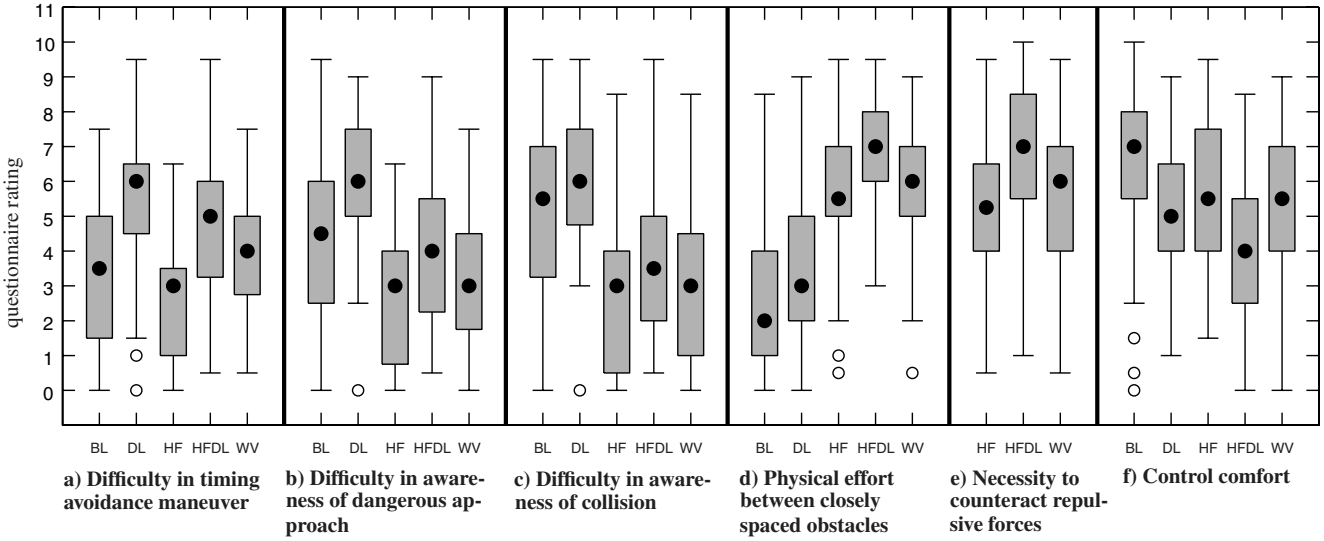

Fig. 19 Medians and interquartile ranges of the answers to the questionnaire with medium (○) outliers.

VII. Discussion

The control theoretical analysis showed that when time delays are involved in a master–slave system, the closed-loop response of the slave can become badly damped or even unstable. A further investigation with a teleoperated rate-command UAV confirmed that manual control would indeed become very difficult. Particularly, flying in a closely spaced, obstacle-laden environment resulted in oscillatory motion and collisions. The application of wave variables to a rate-command control of a UAV, the focus of this study, was shown to be successful. The UAV motion did not show any oscillations and no collisions occurred. In fact, the response was equivalent to the situation without time delays.

A human-in-the-loop experiment confirmed these findings. With haptic feedback, the number of collisions reduced considerably, at the cost, however, of higher operator control activity and workload, which confirms our first hypothesis. However, when regarding teleoperation with time delays, performance deteriorated significantly (in particular, with haptic feedback). Here, the number of collisions, operator control activity, haptic activity, and operator workload all increased, confirming our second hypothesis. The number of collisions remained smaller, however, than in the conditions without any haptic feedback; this result was not significant.

As was hypothesized, the use of wave variables resulted in a significant reduction in the number of collisions, control activity, and operator workload when compared with the situation of haptic feedback with time delay. Operator performance and control activity were restored to the levels of haptic feedback without delay.

The reduction in the time-delay effects can be attributed to the feedback of the repulsive force F_s to the slave at the remote site, block III in Fig. 3b. In fact, the UAV becomes a semi-autonomous system that responds directly to a part of the repulsive forces from the AFF. When the operator perceives the repulsive forces, the UAV *has already decelerated* or, in other words, has already initiated an avoidance maneuver. Because of this feedback at the remote site, subjects reported perceiving a faster UAV response. However, in spite of the fast UAV response to the human reactions with haptic feedback, operator workload was still higher, due to time delays in the feedforward and visual feedback paths.

The anticipatory behavior of the UAV results in larger distances to obstacles, which in turn leads to smaller variations of the external moment on the control device. The wave-variable technique also leads to a relatively large mean of the external moment, due to the inner-loop feedback of the control deflection at the master site, block I in Fig. 3b. Haptic feedback with time delay, but without wave transformation, results in a larger standard deviation of the external moment, due to the delayed feedback and the lack of anticipation of the UAV. The large standard deviation of the haptic feedback with time delay probably contributes *more* to operator workload than the (on average) larger repulsive forces, due to the use of wave variables. However, this should be further investigated in future work.

Results from the pilot questionnaire show that haptic feedback increases operator situation awareness. Although time delays deteriorate situation awareness, the use of wave variables has a potential to counter this effect. Particularly, the timing of initiating an avoidance maneuver is significantly easier with wave variables. With regard to physical workload, haptic feedback leads to larger physical control efforts and the presence of time delays further increases this effect. Again, the use of wave variables leads to lower physical workload, but overall, the workload remains higher than the situation without time delay. As a result, haptic feedback results in overall better situation awareness and a safer operation, although the workload is higher.

Note that in the present experiment, subjects could continue their flight in spite of a collision: they were not provided with any information as to whether or when a collision occurred, nor was there any penalty. It would be interesting to investigate the effects of introducing such a penalty, for instance, by pausing the experiment for a few minutes every time a collision occurred. Tentatively, this would result in more frustration of the operators, increasing their workload (for the configurations without haptic feedback in particular, because the number of collisions will be higher there). Then the resulting workload levels might even be higher than with haptic feedback and wave variables. It is important to investigate whether operators indeed become more appreciative of the haptic feedback when it helps them to prevent collisions, despite the higher physical workload.

Finally, in this research, haptic feedback was implemented as a classical force feedback (i.e., using a force offset on the stick). In recent research, it was found that an alternative method, so-called stiffness feedback, can reduce physical workload considerably [17]. It would therefore be interesting to investigate the effectiveness of using wave variables when using this stiffness feedback in the presence of time delays.

VIII. Conclusions

Haptic feedback increases operator situation awareness and the safety of teleoperation at the cost of a higher physical workload. With a time delay, however, the number of collisions, operator control activity, and workload all increase and situation awareness deteriorates. Wave-variable transformation is also applicable to a vehicle control that requires rate command. It reduces the time-delay effects significantly and the number of collisions becomes even lower than in the case of haptic feedback without time delay. Operator performance and control activity reach levels similar to

those found with haptic feedback without time delay, but the workload is still higher.

Acknowledgment

The authors thank the Netherlands Agency for Aerospace Programmes (NIVR) for their financial support to this project (NIVR project 49307TU).

References

[1] Monson, C. B., Fong, C. S., Marsh, R. A., and Haas, M. W., "Addressing the Human Element in Unmanned Aerial Vehicles," 36th AIAA Aerospace Sciences Meeting, Reno, NV, AIAA Paper 1998-1032, Jan. 1998, pp. 1–7.

[2] McCarley, J. S., and Wickens, C. D., "Human Factors Implications of UAVs in the National Airspace," Univ. of Illinois at Urbana–Champaign, Aviation Human Factors Div., TR AHFD-05-05/FAA-05-01, Savoy, IL, 2005.

[3] Sheridan, T. B., and Ferrell, W. R., "Remote Manipulative Control with Transmission Delay," *IEEE Transactions on Human Factors in Electronics*, Vol. HFE-4, No. 1, Sept. 1963, pp. 25–29. doi:10.1109/THFE.1963.231283

[4] Sheridan, T. B., "Space Teleoperation Through Time Delay: Review and Prognosis," *IEEE Transactions on Robotics and Automation*, Vol. 9, Oct. 1993, pp. 592–606. doi:10.1109/70.258052

[5] Anderson, R. J., and Spong, M. W., "Bilateral Control of Teleoperators with Time Delay," *IEEE Transactions on Automatic Control*, Vol. 34, No. 5, May 1989, pp. 494–501. doi:10.1109/9.24201

[6] Lee, S., Sukhatme, G. S., Kim, G. J., and Park, C., "Haptic Control of a Mobile Robot: A User Study," *Proceedings of the 2002 IEEE/RSJ International Conference on Intelligence Robots and Systems*, Vol. 3, Inst. of Electrical and Electronics Engineers, Piscataway, NJ, 2002, pp. 2867–2874.

[7] Lim, J., Ko, J., and Lee, J., "Internet-Based Teleoperation of a Mobile Robot with Force-Reflection," *Proceedings of the 2003 IEEE Conference on Control Applications*, Vol. 1, Inst. of Electrical and Electronics Engineers, Piscataway, NJ, 23–25 June 2003, pp. 680–685.

[8] Xiao, D., and Hubbold, R., "Navigation Guided by Artificial Force Fields," *Human Factors in Computer Systems: Making the Impossible Possible*, Association for Computing Machinery, New York, 18–23 Apr. 1998, pp. 179–186.

[9] Elhajj, I., Xi, N., Fung, W. K., Liu, Y. H., Li, W. J., Kaga, T., and Fukuda, T., "Haptic Information in Internet-Based Teleoperation," *IEEE/ASME Transactions on Mechatronics*, Vol. 6, No. 3, Sept. 2001, pp. 295–304. doi:10.1109/3516.951367

[10] Repperger, D. W., Chandler, A. P., and Chelette, T. L., "A Study on Spatially Induced 'Virtual Force' with an Information Theoretic Investigation of Human Performance," *IEEE Transactions on Systems, Man, and Cybernetics*, Vol. 25, No. 10, Oct. 1995, pp. 1392–1404. doi:10.1109/21.464442

[11] Repperger, D. W., Phillips, C. A., and Washington, K. R., "A Study on Stable Teleoperation with Time Delays and Haptic Interfaces," *Proceedings of the Ninth IFAC/IFIP/IFORS/IEA Symposium on Analysis, Design and Evaluation of Man–Machine Systems* [CD-ROM], Georgia Inst. of Technology, Atlanta, Sept. 2004.

[12] Hannaford, B., Wood, L. P., McAffee, D. A., and Zak, H., "Performance Evaluated of a Six-Axis Generalized Force-Reflecting Teleoperator," *IEEE Transactions on Systems, Man, and Cybernetics*, Vol. 21, No. 3, May–June 1991, pp. 620–633. doi:10.1109/21.97455

[13] Lam, T. M., Mulder, M., and van Paassen, M. M., "Haptic Interface for UAV Collision Avoidance," International Journal of Aviation Psychology, Vol. 17, No. 2, 2007, pp. 167–195.

[14] Boschloo, H. W., Lam, T. M., Mulder, M., and van Paassen, M. M., "Collision Avoidance for a Remotely Operated Helicopter Using Haptic Feedback," *IEEE International Conference on Systems Man and Cybernetics*, Inst. of Electrical and Electronics Engineers, Piscataway, NJ, 10–13 Oct. 2004, pp. 229–235.

[15] Lam, T. M., Boschloo, H. W., Mulder, M., and van Paassen, M. M., "Artificial Force Field for Collision Avoidance in the UAV Teleoperation," *IEEE Transactions on Systems Man and Cybernetics* (to be published).

[16] Lam, T. M., Boschloo, H. W., Mulder, M., van Paassen, M. M., and van der Helm, F., "Effect of Haptic Feedback in a Trajectory Following Task with an Unmanned Aerial Vehicle," *IEEE International Conference on Systems Man and Cybernetics*, Inst. of Electrical and Electronics Engineers, Piscataway, NJ, Oct. 2004, pp. 2500–2506.

[17] Lam, T. M., Mulder, M., and van Paassen, M. M., "Haptic Feedback for UAV Teleoperation—Force Offset and Spring Load Modification," *IEEE International Conference on Systems Man and Cybernetics*, Inst. of Electrical and Electronics Engineers, Piscataway, NJ, Oct. 2006, pp. 1618–1623.

[18] Lam, T. M., V., D., Mulder, M., and van Paassen, M. M., "UAV Teleoperation Using Haptics with a Degraded Visual Interface," *IEEE International Conference on Systems Man and Cybernetics*, Inst. of Electrical and Electronics Engineers, Piscataway, NJ, Oct. 2006, pp. 2440–2445.

[19] Ferrell, W. R., "Remote Manipulation with Transmission Delay," *IEEE Transactions on Human Factors in Electronics*, Vol. 6, 1965, pp. 24–33.

[20] Tanner, N. A., and Niemeyer, G., "Online Tuning of Wave Impedance in Telerobotics," *Proceedings of IEEE Conference on Robotics, Automation, and Mechatronics*, Vol. 1, Inst. of Electrical and Electronics Engineers, Piscataway, NJ, Dec. 2004, pp. 7–12.

[21] Anderson, R. J., and Spong, M. W., "Bilateral Control of Teleoperators with Time Delay," *Proceedings of the 27th IEEE Conference on Decision and Control*, Inst. of Electrical and Electronics Engineers, Piscataway, NJ, 1988, pp. 167–173.

[22] Niemeyer, G., and Slotine, J. J. E., "Stable Adaptive Teleoperation," *IEEE Journal of Oceanic Engineering*, Vol. 16, No. 1, Jan. 1991, pp. 152–162. doi:10.1109/48.64895

[23] Niemeyer, G., and Slotine, J. J. E., "Telemanipulation with Time Delays," *The International Journal of Robotics Research*, Vol. 23, No. 9, Sept. 2004, pp. 873–890. doi:10.1177/0278364904045563

[24] Tanner, N. A., and Niemeyer, G., "Improving Perception in Time Delayed Teleoperation," *Proceedings of the 2005 IEEE Conference on Robotics and Automation*, Vol. 1, Inst. of Electrical and Electronics Engineers, Piscataway, NJ, Apr. 2005, pp. 354–359.

[25] Niemeyer, G., and Slotine, J. J. E., "Towards Force-Reflecting Teleoperation over the Internet," *Proceedings of the 1997 IEEE International Conference on Robotics and Automation*, Inst. of Electrical and Electronics Engineers, Piscataway, NJ, May 1998, pp. 1909–1915.

[26] Yokokohji, Y., Imaida, T., and Yoshikawa, T., "Bilateral Teleoperation Under Time-Varying Communication Delay," *IEEE/RSJ International Conference on Intelligent Robotics and Systems*, Inst. of Electrical and Electronics Engineers, Piscataway, NJ, 1999, pp. 1854–1859.

[27] Munir, S., and Book, W. J., "Internet-Based Teleoperation Using Wave Variables with Prediction," *IEEE/ASME Transactions on Mechatronics*, Vol. 7, No. 2, June 2002, pp. 124–133. doi:10.1109/TMECH.2002.1011249

[28] Dede, M. I. C., Tosunoglu, S., and Repperger, D. W., "Effects of Time Delay on Force-Feedback Teleoperation Systems," *Proceedings of the IEEE/CSS 12th Mediterranean Conference on Control Automation*, Inst. of Electrical and Electronics Engineers, Piscataway, NJ, June 2004, pp. 6–9. doi:10.1109/ICMECH.2004.1364485

[29] Dede, M. I. C., Tosunoglu, S., and Repperger, D. W., "A Study on Multiple Degree-of-Freedom Force Reflecting Teleoperation," *Proceedings of the IEEE International Conference on Mechatronics (ICM '04)*, Inst. of Electrical and Electronics Engineers, Piscataway, NJ, June 2004, pp. 476–481.

[30] Niemeyer, G., "Using Wave Variables in Time Delayed Force Reflecting Teleoperation," Ph.D. Dissertation, Massachusetts Inst. of Technology, Cambridge, MA, 1996.

[31] Lew, J. Y., and Repperger, D. W., "Wave Variables Based Teleoperation with Time Delay: Application to Space Based Laser Maintenance," *IEEE Aerospace Conference Proceedings*, Vol. 5, 6–13 Mar. 2004, pp. 2912–2919.

[32] Hannaford, B., and Ryu, J.-H., "Time-Domain Passivity Control of Haptic Interfaces," *IEEE Transactions on Robotics and Automation*, Vol. 18, No. 1, Feb. 2002, pp. 1–10. doi:10.1109/70.988969

[33] Hart, S. G., and Staveland, L. E., "Development of NASA-TLX (Task Load Index): Results of Empirical and Theoretical Research," *Human Mental Workload*, edited by P. A. Hancock and N. Meshkati, North-Holland, Amsterdam, 1988, pp. 139–183.

[34] Voorsluijs, G. M., Bennani, S., and Scherer, C. W., "Linear and Parameter-dependent Robust Control Techniques Applied to a Helicopter UAV," 38th AIAA Guidance, Navigation and Control Conference, Providence, RI, AIAA Paper 2004-4909, Aug. 2004, pp. 1–11.